

Parachute deployment simulations using LS-DYNA ICFD solver and strong FSI coupling

Morgan LE GARREC¹, Arnaud PONCET¹, Vincent LAPOUJADE¹

¹DynaS+, Toulouse, France

1 Introduction

The main goal of military airdrops is the accurate delivery of cargo released from a moving air vehicle via parachute. The airdrop trajectory results from the movement of the dropped package and the dynamics of the parachutes deployment (Fig.1:). After having treated the freefall of a rigid object in the near flow of an airplane ([8]), the present paper focuses on the parachute deployment modelling and its challenges in LS-DYNA.

In preliminaries, the main characteristics of the test case parachute are described. Then the folding procedure is briefly discussed. Calibration of the structural part is performed separately, mostly focusing on the implicit dynamics scheme. Finally, FSI calculations are run, with increasing complexity:

- On the reference deployed geometry with a constant inlet velocity,
- On a semi-folded state in the parachute reference frame,
- Adding permeability on the parachute surface.

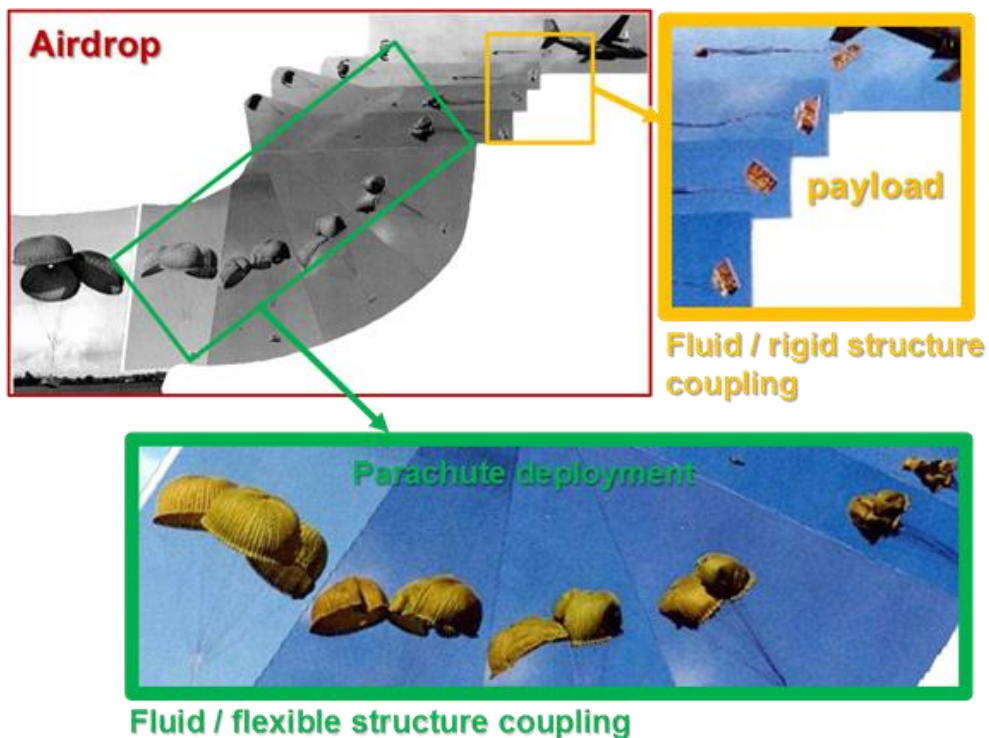


Fig.1: Highlighting of two types of fluid-structure interactions during airdrop

2 Preliminary: Parachute and materials description

2.1 Parachute model description

The parachute model used for the present study is a 2m in diameter hemispherical parachute, using only one fabric for its canopy panels. Each panel is bordered by ribbons, and there are 14 rigging lines attached to a rigid straight bar at the bottom.

All fabric parts are modelled using shell elements, including the ribbons. The lines are modelled using beam cable elements.

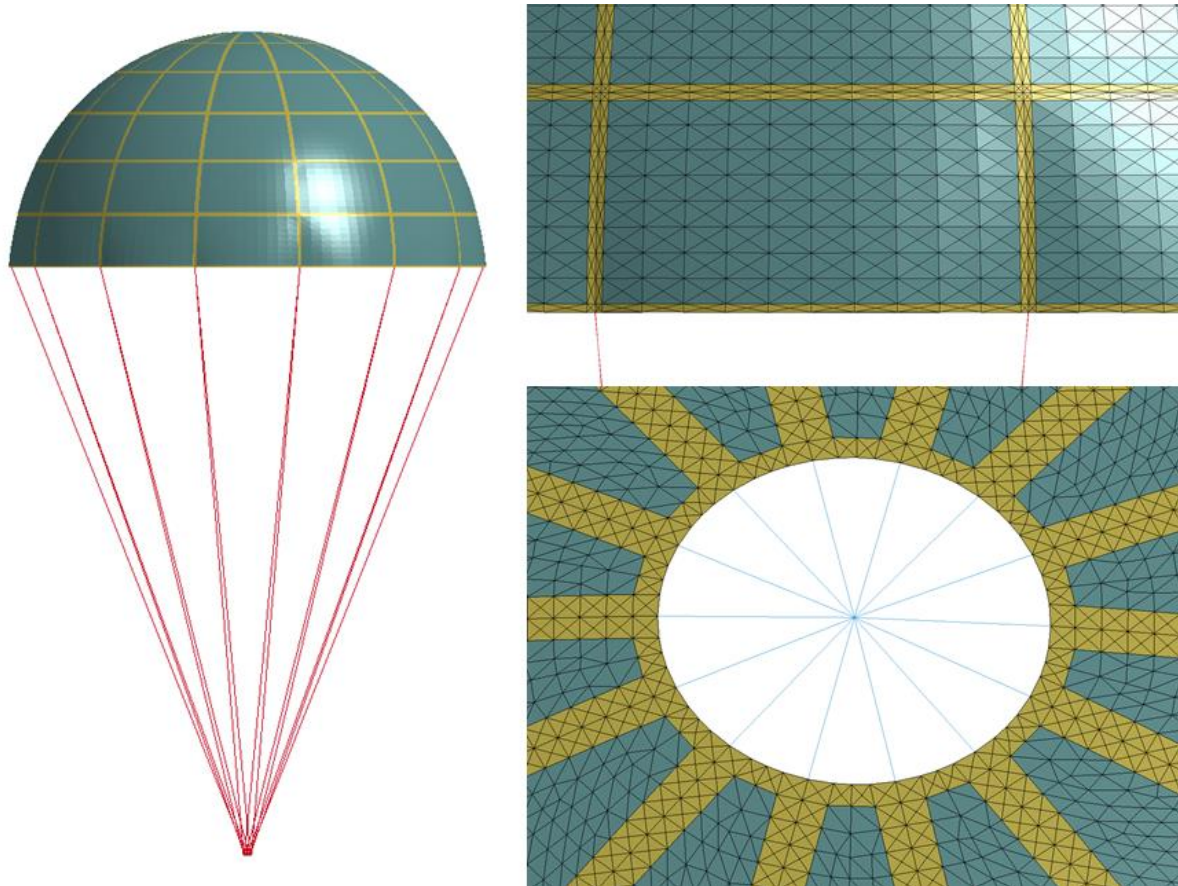


Fig.2: Test case parachute mesh in deployed configuration

2.2 Material characterization

During the initial phase of PARAFLU project, a test campaign was conducted on various fabrics present in the French military parachutes. An extensive material characterization was performed, with uniaxial tension tests, biaxial tension tests, and permeability measurements in unloaded state as well as in biaxially tensile state.

These results were then used in LS-Opt for identification of *MAT_FABRIC parameters, in both linear and non-linear behavior.

2.3 *MAT_FABRIC parametrization

The various element formulations included in the MAT_34 need specific handling in each case. Because the ultimate aim is to use non-linear biaxial stress/strain curves, the mapped version of the material, *MAT_FABRIC_MAP, is preferred. It allows the use of the compressive stress elimination routine, as well as the addition of coating to the fabric in order to stiffen the material in compression and flexion.

For the present paper however, the *MAT_FABRIC formulation 12 was used because it is easier to handle and is sufficient for the feasibility of the modelled problem.

3 Folding procedure

3.1 Description of the strategies

The parachute is folded directly in LS-DYNA using heavily mass-scaled and damped simulations, as well as rigid tools. Several steps are performed with a different input deck each time. Because of prestressing issues, each step terminates with a long period of time without any external loads or constraints applied: this ensures that the folded geometry does not generate excessive initial stresses when calling the reference geometry.

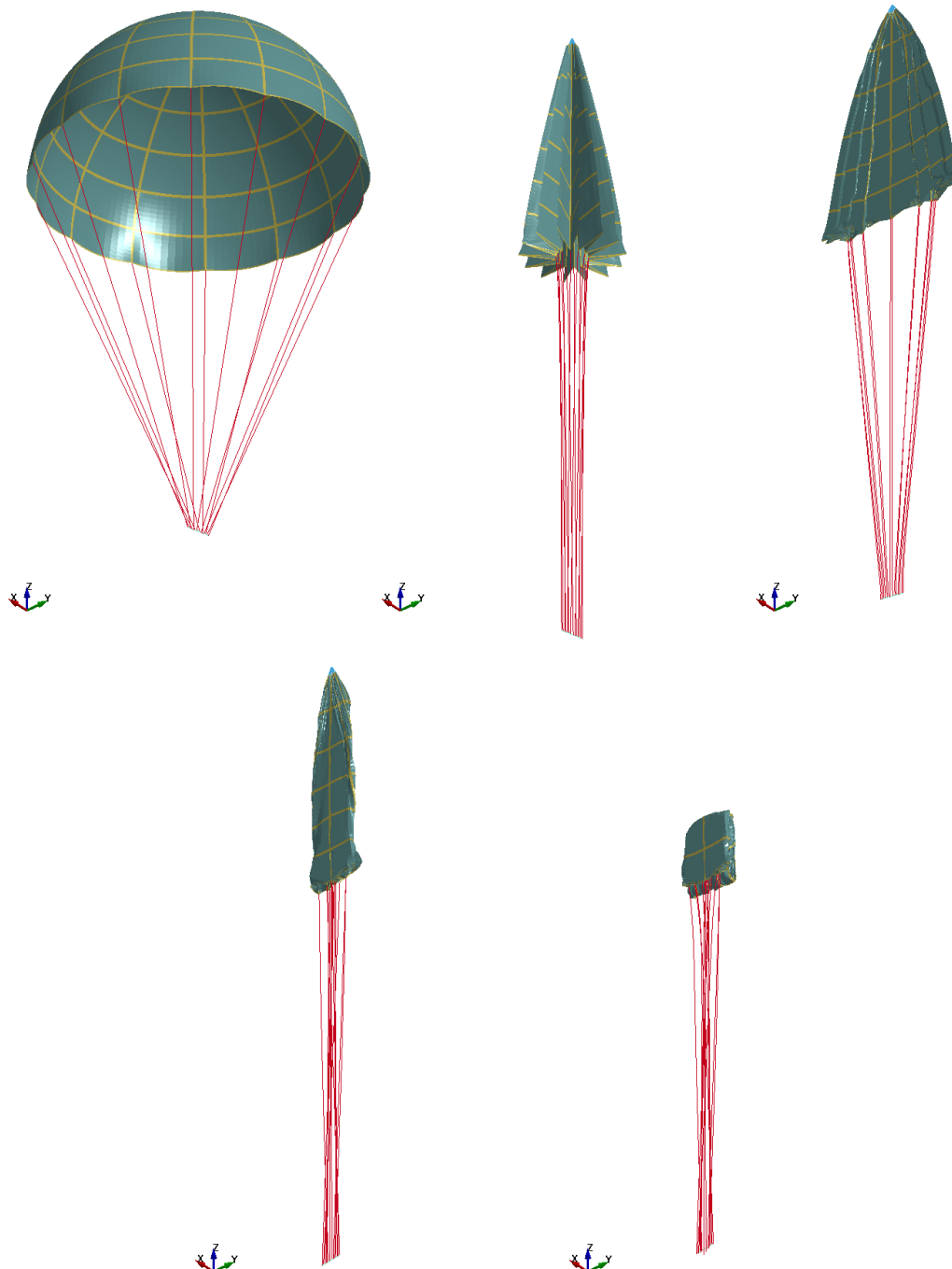


Fig.3: Folding steps

3.2 Remeshing for the coupled ICFD surface

In order to control the ICFD mesh size in the parachute vicinity, a remeshing of the folded geometry is performed. Care is taken in subsequent FSI analyses to loosen the coupling tolerance in order to find suitable host nodes because of the non-coincident mesh between the structural and fluid surfaces.

Two different configurations were used for the ICFD calculations: the first one is the reference geometry, and the second one is an intermediate “semi-folded” configuration. Its geometry was extracted from the pressure deployment and run with no loads in order to balance the internal forces. The “pinetree” geometry could not lead to successful ICFD meshing for the present paper.

The applied mesh size on the ICFD surface coupled with the structure is 20-50 mm. The meshes are the following for both configurations:

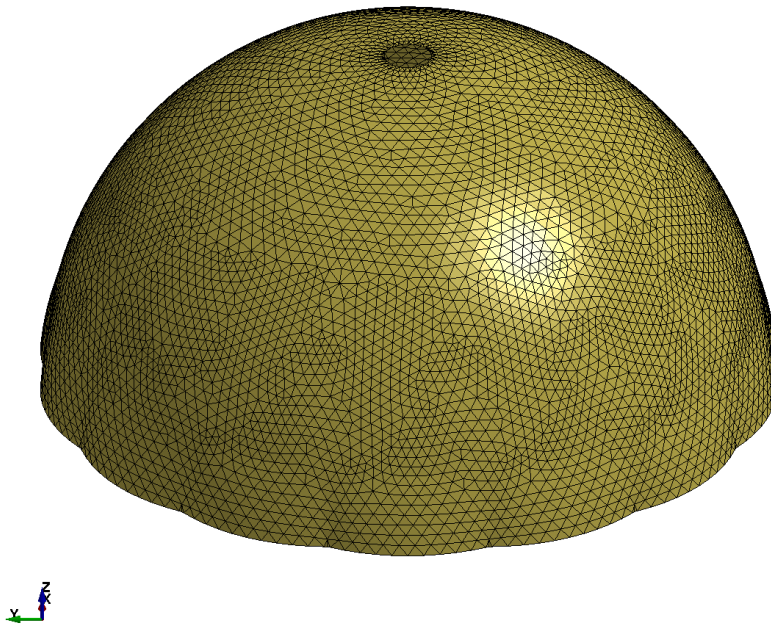


Fig.4: ICFD mesh in reference configuration

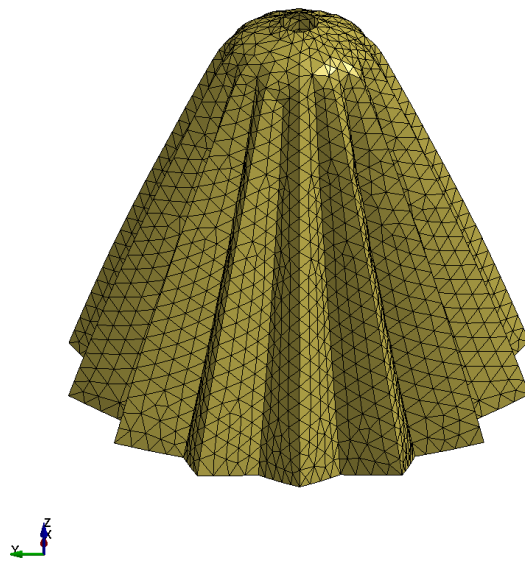


Fig.5: ICFD mesh in semi-folded configuration

4 Deployment in lagrangian dynamics only

4.1 Application of a representative pressure loading

In order to model the same dynamics as for an actual deployment, the following assumption is made: the flow inside the parachute is stationary while outside it has the same velocity as the parachute itself. From actual drop test cases, this velocity typically ranges from 40m/s to 4m/s over a duration of 0.5s.

From Bernoulli's equation, we can link the velocity to the pressure difference between both parachute faces:

$$p = p_0 + \frac{1}{2} \rho_{air} u^2 \quad (1)$$

With:

- $p_0 = 0$ arbitrarily chosen,
- $\rho_{air} = 1.225 \text{kg/m}^3$ the air density,
- u the fluid velocity.

The resulting pressure signal ranges from 0 Pa (prior to bag exit), to a shock of 1000 Pa over 100ms, to a progressive diminution to 10 Pa over 500ms:

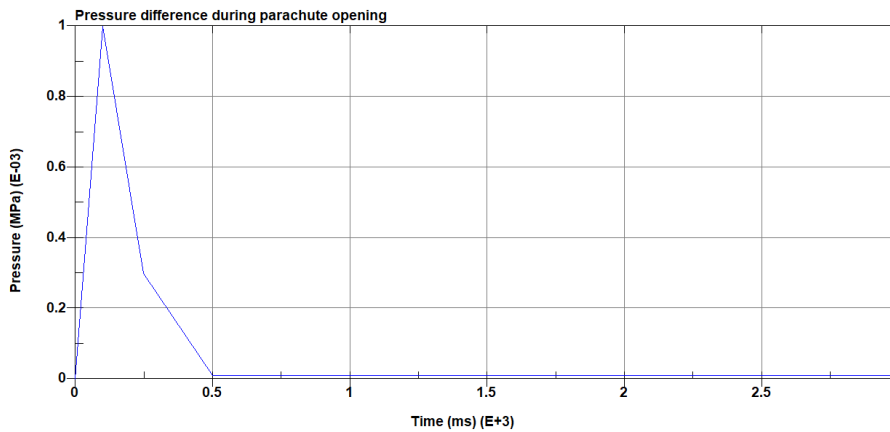


Fig.6: Pressure signal applied to the folded parachute for pure lagrangian opening

This loading is first tested on an explicit simulation in order to verify the fabric behavior. The model is clamped by its rigid bar at the bottom, and the apex is kept in its horizontal plane while still being allowed to move vertically. This last boundary condition, although non-physical, improves the global stability of these preliminary calculations.

Wrinkles can be seen in the fabric during deployment, which could cause some issues when switching to implicit calculations. In addition, the folds tend to touch each other, necessitating a thorough contact management, including the choice of a contact thickness allowing for large enough gaps for the ICFD mesher.

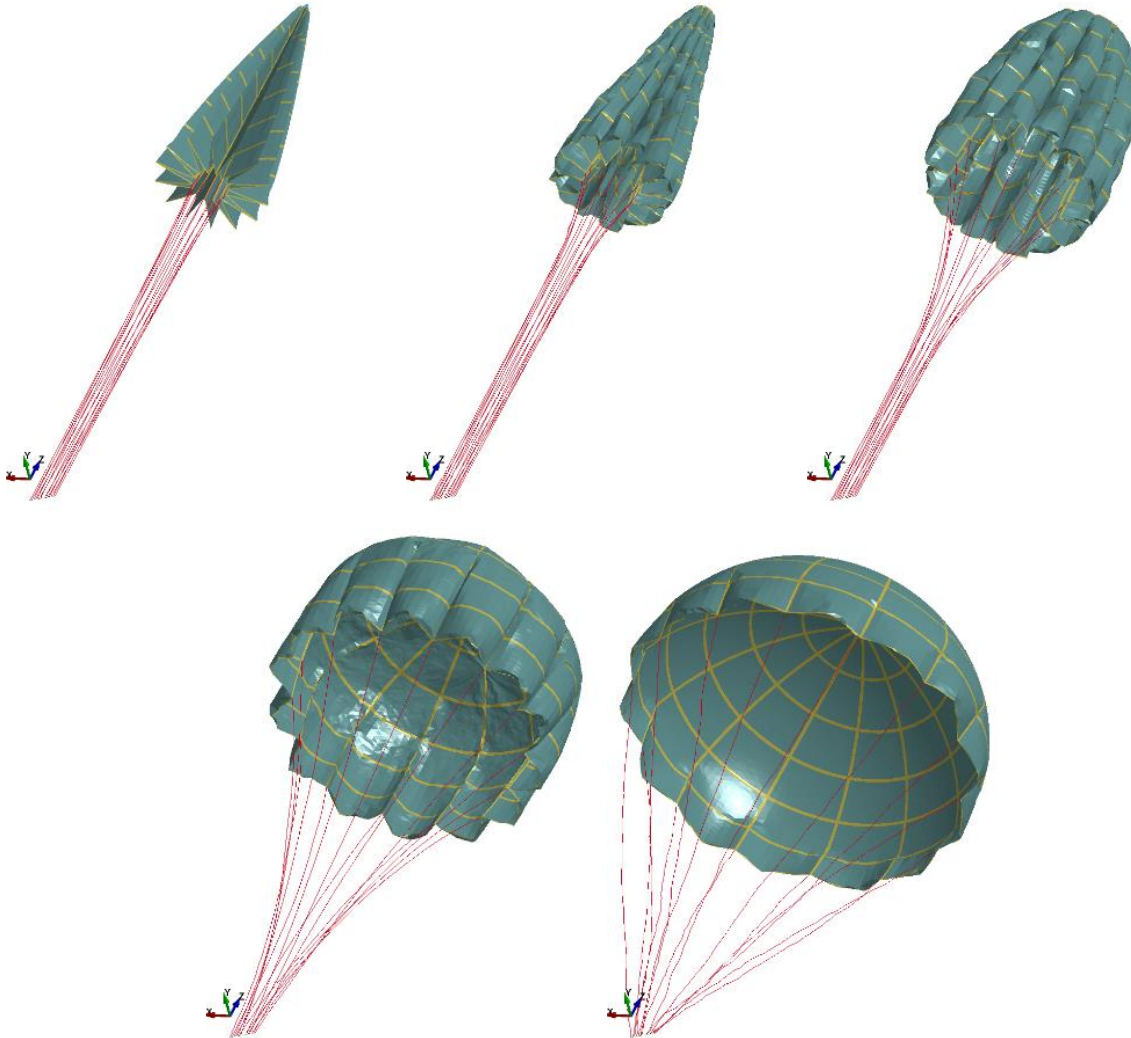


Fig.7: Parachute opening during explicit calculation using a pressure load

4.2 Implicit parametrization

The implicit solver uses high numerical damping in the Newark model ($\gamma = 0.6$, $\beta = 0.38$). Convergence criteria are slightly relaxed ($dctol = 0.002$, $ectol = 0.02$), but the displacement norm is calculated based on the initial displacement from the current step rather than from the full displacement. This latter assumption is important with highly deformable parts, more so when it is planned to let them fall freely in a general frame.

The time step is chosen so as to balance the number of iterations at each step and the total number of steps in the simulation. It was fixed at 1ms for the present calculation.

The implicit scheme tends to filter high frequency phenomena. The reaction force time history at the bottom of the lines is monitored as a comparison between both schemes. It can be seen in Fig.9: and shows the same signal in explicit and implicit, although smoother for the implicit force.

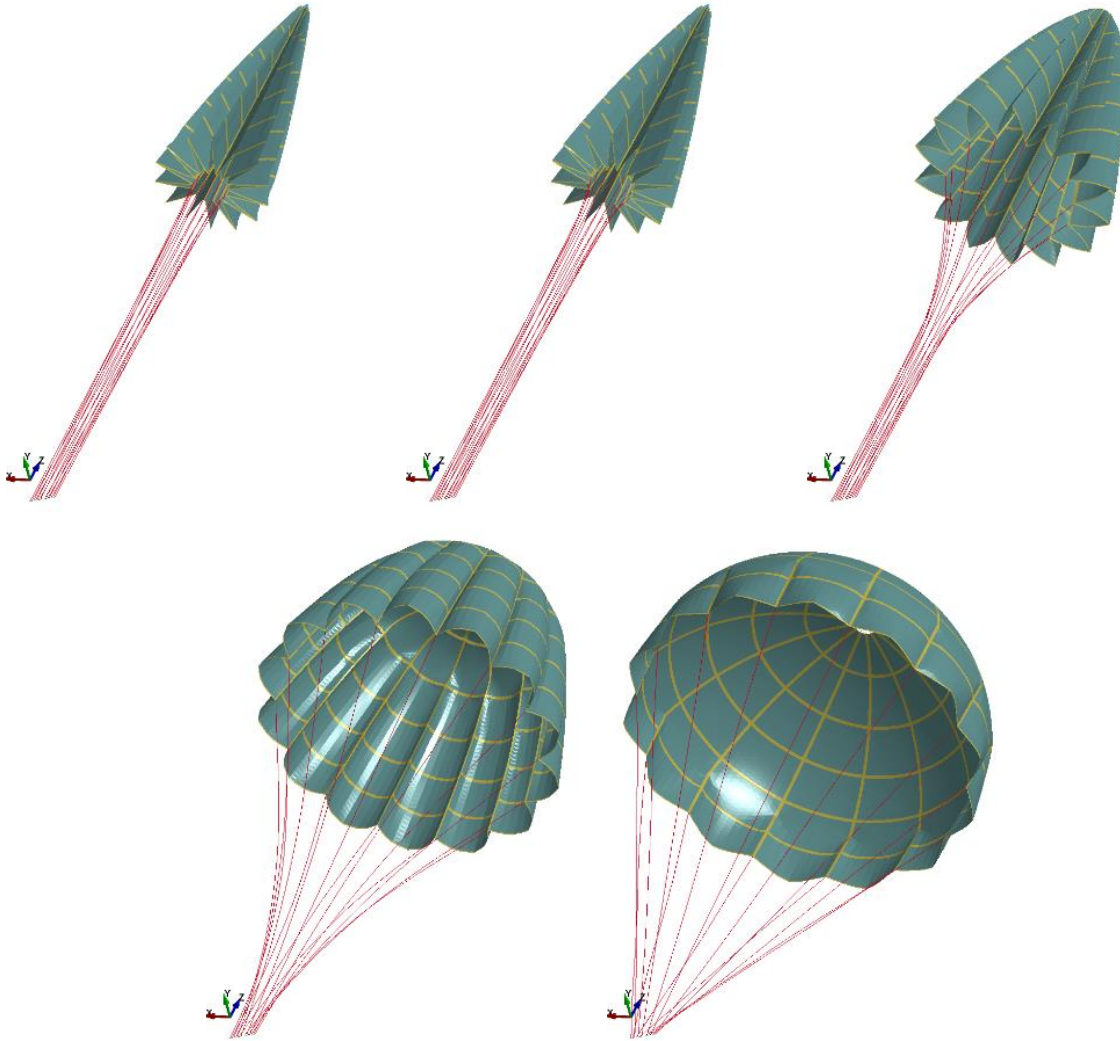


Fig.8: Parachute opening during implicit dynamics calculation using a pressure load

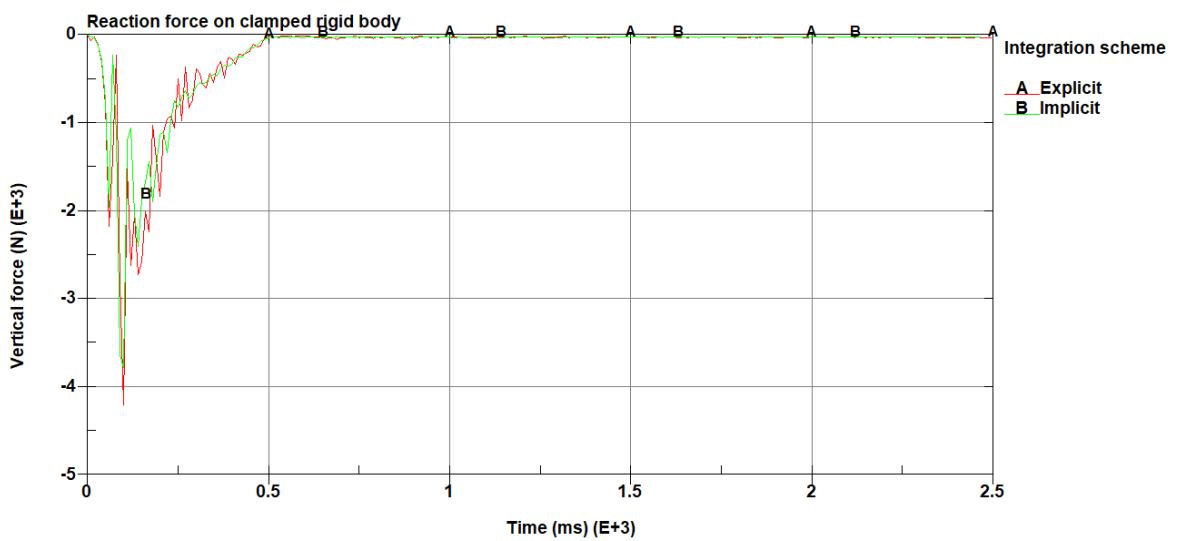


Fig.9: Clamp force comparison between explicit and implicit schemes

5 FSI calculations

All FSI calculations were run using a default LES turbulence model. A refined sphere centered around the parachute with a 2.4m diameter is defined. The domain is a cylinder with a 10m diameter and a 50m height. Its boundaries are meshed using an unstructured 1-2m triangular mesh.

5.1 FSI calculation on the reference geometry

The reference geometry is used in order to assess the model size with the elected remeshing size at the parachute surface and the refinement zone around it. A reference drag is also computed. Two cases are run: the first one with the ICFD mesh surface shown in Fig.4., and the second one with a surface mesh matching the structural mesh.

A constant velocity of 5 m/s is applied at the inflow of the model. After validation runs using only the fluid part, coupled calculations are run. Drag time history shows similar behavior with both meshes:

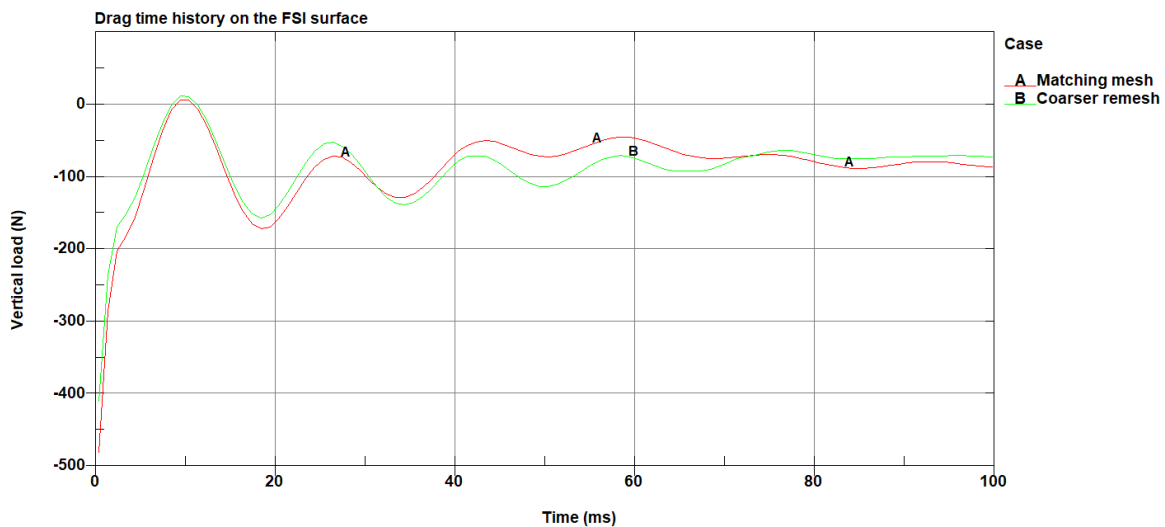


Fig.10: Drag force acting on the FSI surface with constant inflow velocity

The load shows a shock response corresponding to the development of the flow around the parachute. This signal is quickly damped and around 80 ms of simulation, oscillations become small. The stabilized drag is 89 N. The drag coefficient is calculated as follows:

$$C_d = \frac{F_z}{\frac{1}{2} \rho_{air} S u^2} = 1.85 \quad (2)$$

With:

- $S = 3.14\text{m}^2$ the parachute projected surface,
- $F_z = 89\text{N}$ the measured drag load,
- $u = 5\text{m/s}$ the fluid velocity.

This value is slightly higher than the usually assumed drag coefficient applying for a hollow half sphere of 1.42 (ref. [9]).

Fig.11: shows the flow around the parachute after stabilization, as well as stress in the parachute. Eddy generation can be seen on the outer surface.

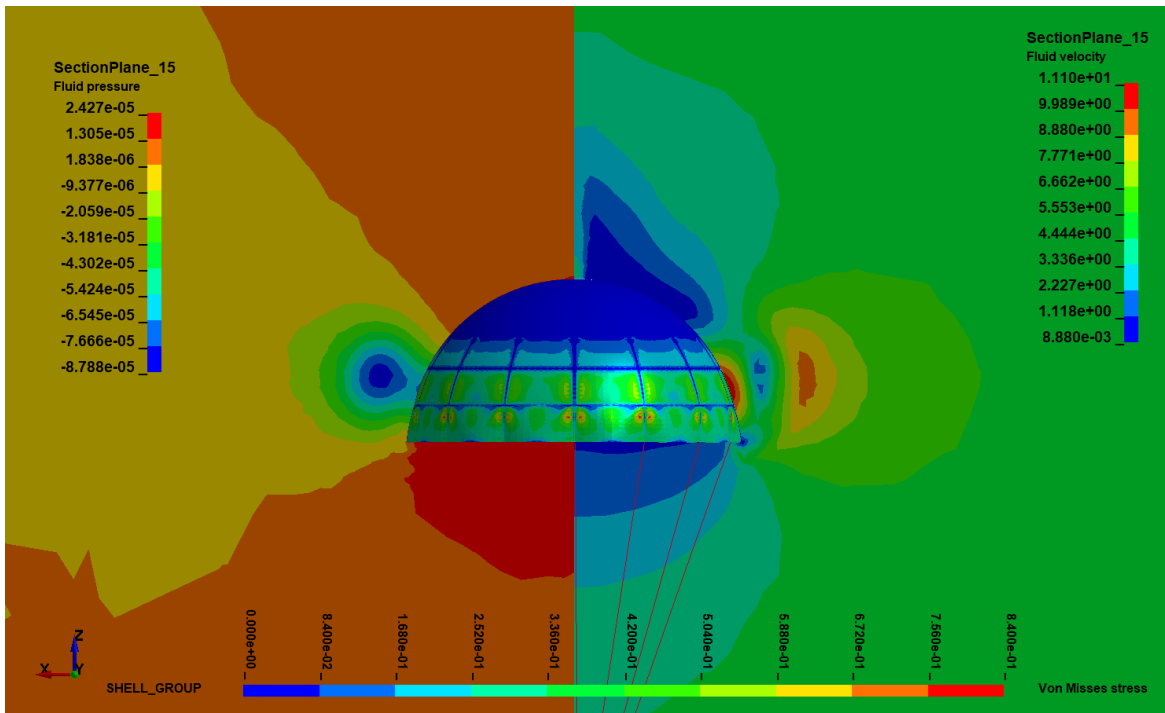


Fig.11: Pressure and velocity fields after stabilization

5.2 Permeability implementation

5.2.1 Permeability on thin structures

The ICFD solver historically allowed to define porous domains using a volume definition. It is now possible to apply permeability equations through thin structures, generally represented as a single ICFD surface using the mesh embedment functionality (*ICFD_MESH_EMBEDSHELL).

The porous material is called by the ICFD surface, and the actual fabric thickness is needed when defining the permeability parameters. The porous embedded shell in itself constitutes a domain boundary condition, so the user must not define any additional no-slip condition on the surface.

For the present case, an Ergun model was chosen, with a porosity of 1.0 and a permeability of 0.0001 mm².

5.2.2 Comparison of flows around reference geometry

The reference geometry case was run using a porous media in replacement to the no-slip wall on the parachute surface. Because the reference geometry only shows small deformations during the FSI calculations, the structural part was excluded from this comparison. This permitted to save computational time.

The velocity field clearly shows the leakage through the surface, in the order of 1m/s. The comparison with and without porous medium can be seen in Fig.12:.

The pressure drop between both faces of the parachute is also reduced, with only around 20Pa instead of 38Pa. The comparison can be seen in Fig.13:.. The drag time history shows a reduced load acting on the parachute, with a stabilized drag load of only 54N acting on the surface. This corresponds to nearly 40% loss of drag, as show in §5.1. It has to be noted that the permeability was arbitrarily chosen and an actual measured value could be lower. For instance, the same computation with 50% of the initial permeability leads to a stabilized drag of 61N.

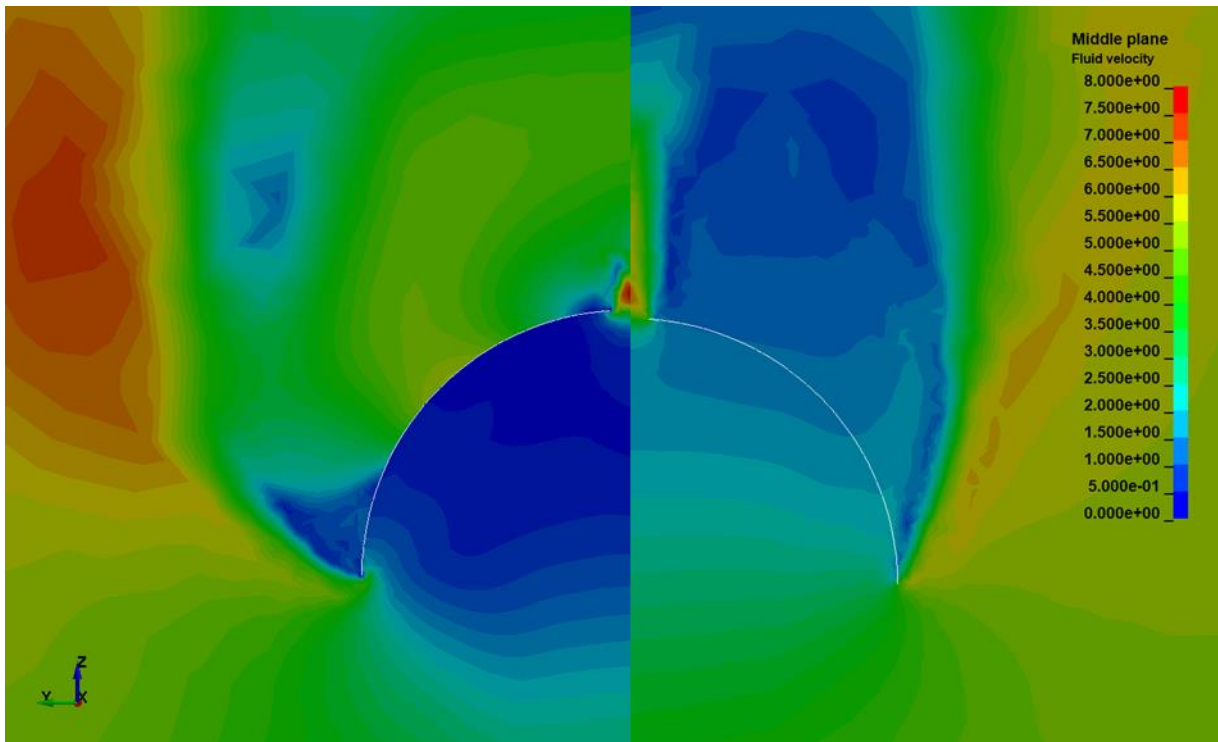


Fig.12: Velocity field without (left) et with (right) permeability

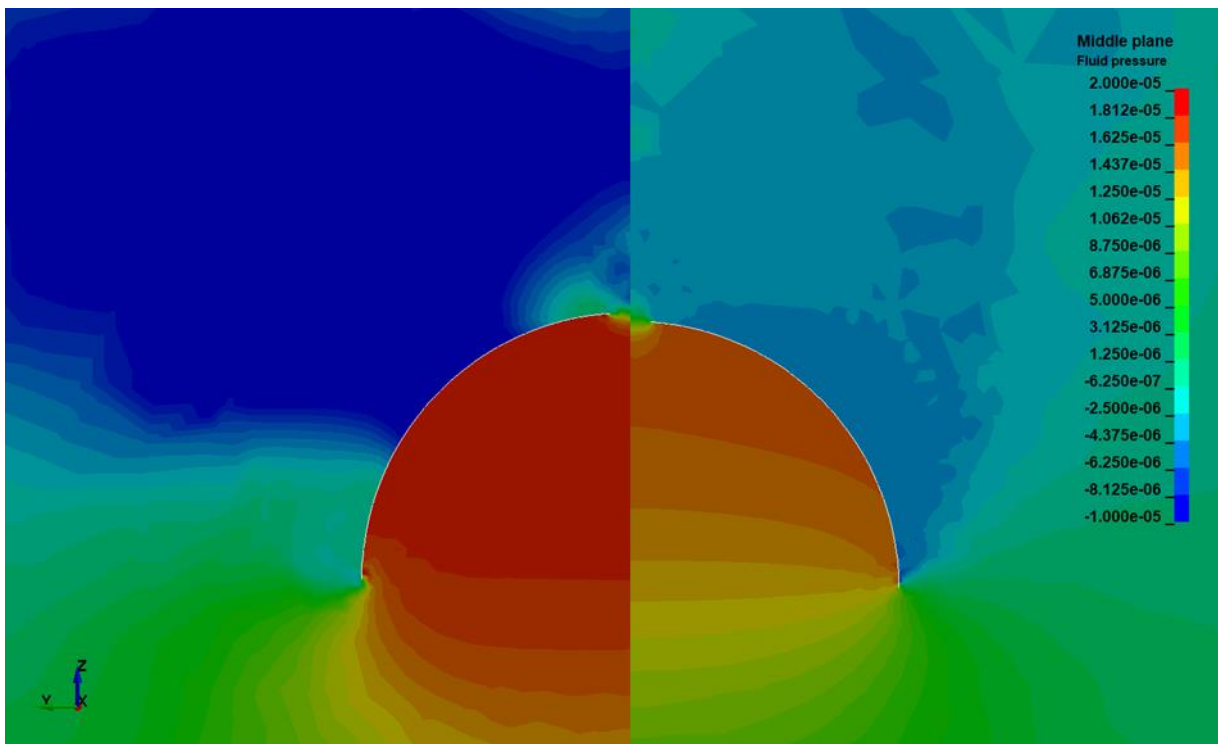


Fig.13: Pressure field without (left) et with (right) permeability

5.3 FSI deployment calculations in the parachute reference frame

The semi-deployed configuration was retained for these calculations. A constant inlet velocity of 5m/s is applied to the parachute, with the rigid bar fixed in all directions. The coupling is applied after 2ms in order to generate the velocity and pressure fields. The parachute shows similar behavior as for the pressure application described in §4.2.

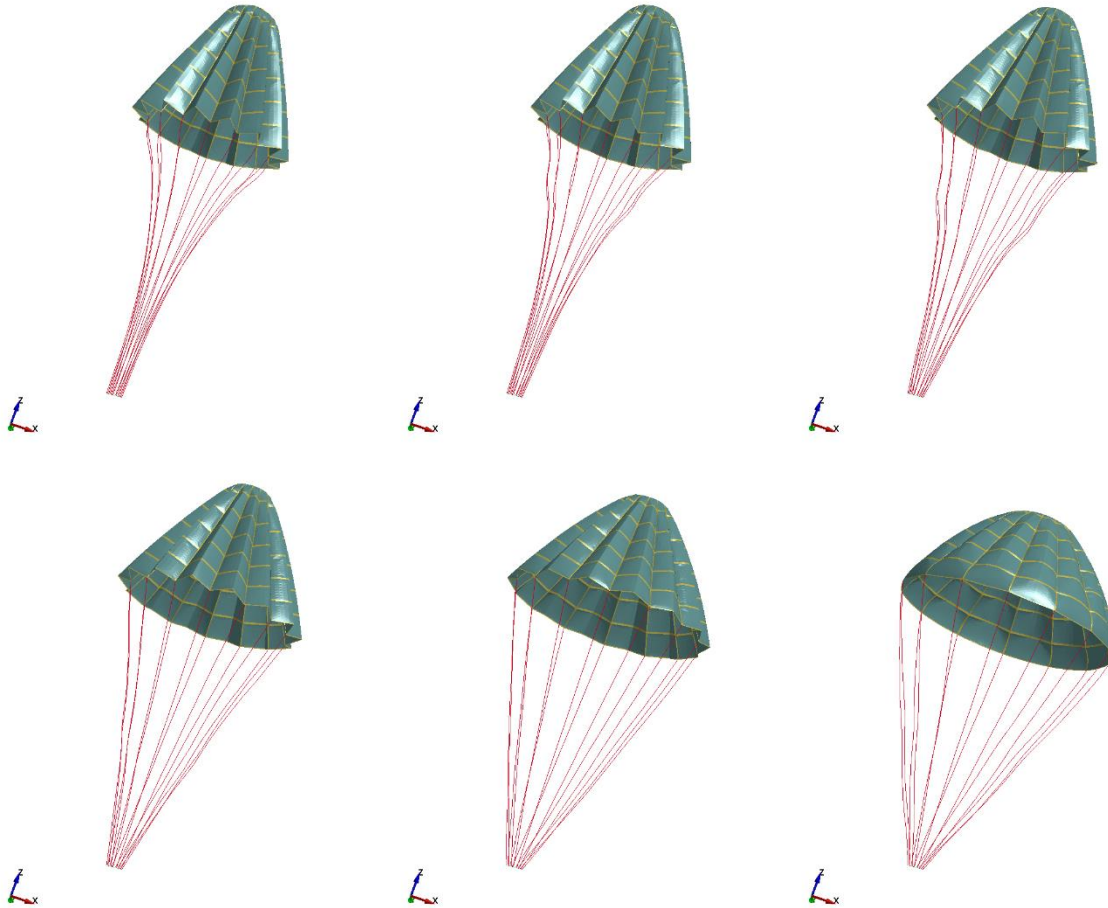


Fig. 14: FSI deployment of parachute every 40ms from semi-deployed configuration

The vertical load time history shows large amounts of noise but the final average load is around 100N, as also shown in 5.1.

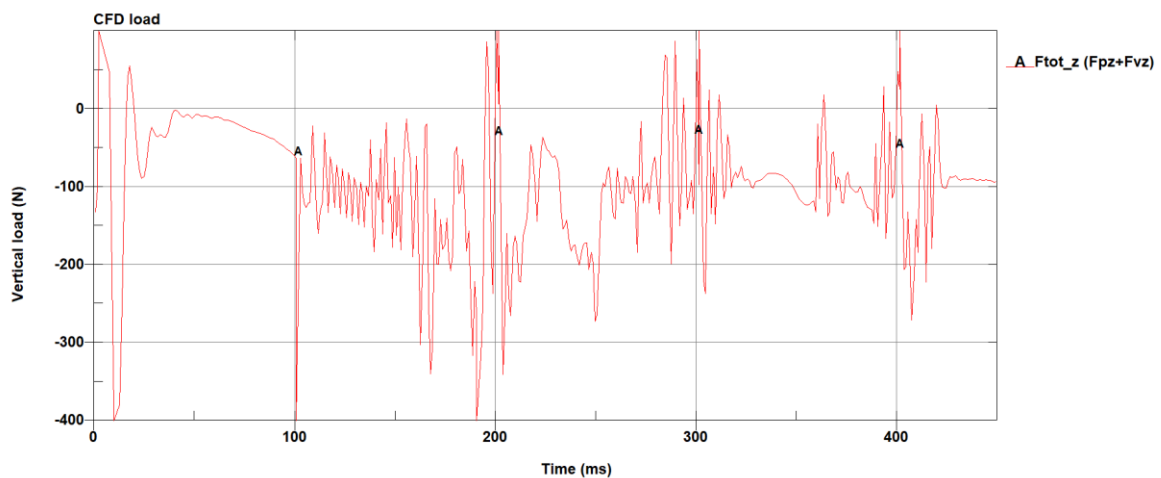


Fig. 15: FSI deployment vertical load time history

The flow in and around the parachute shows the pressure difference leading to the deployment. Eddies are visible at the edge of the panels, as well as above the apex, where some of the flow is regularly released.

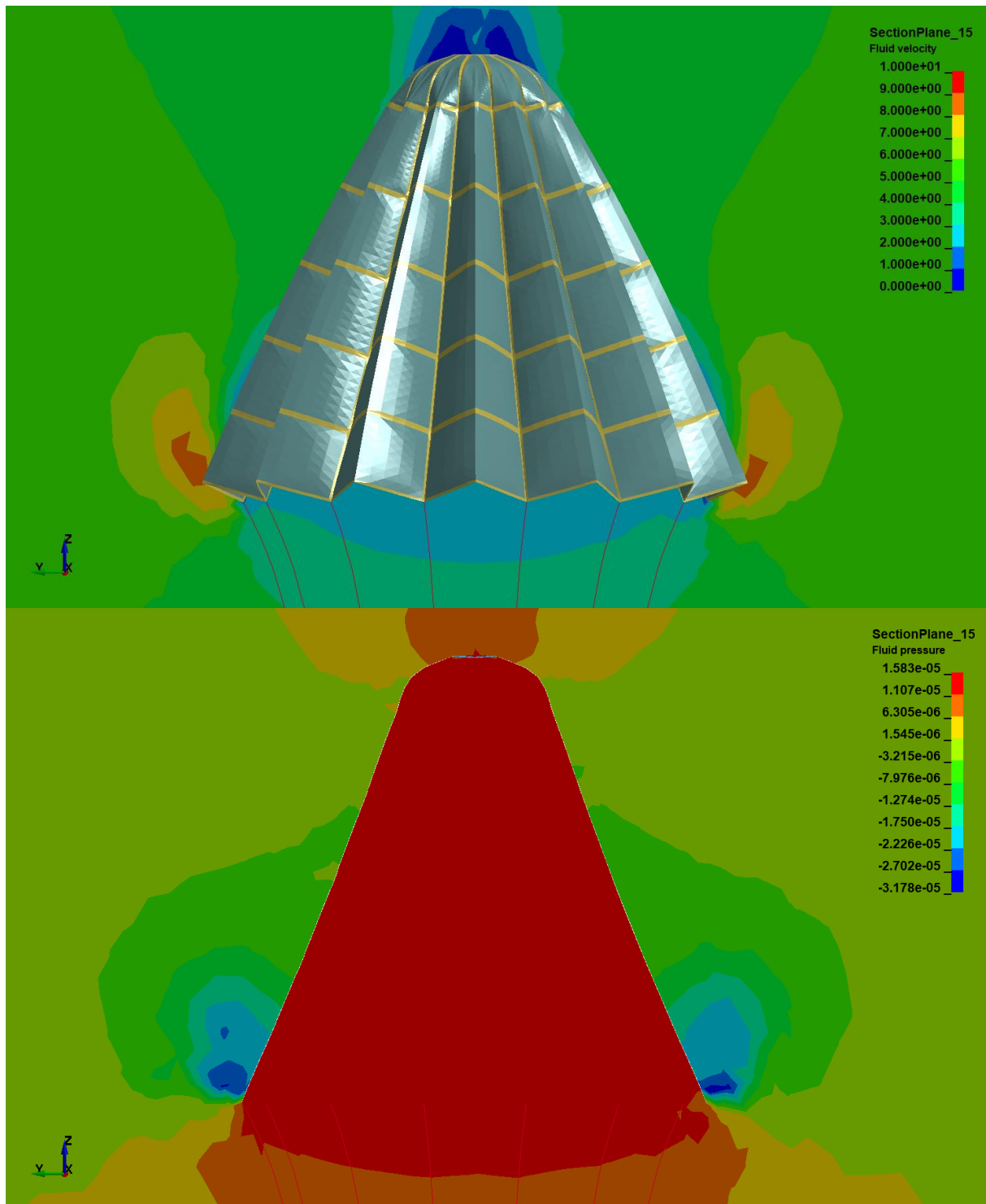


Fig.16: Velocity (top) and pressure (bottom) fields during FSI deployment at $t=80\text{ms}$

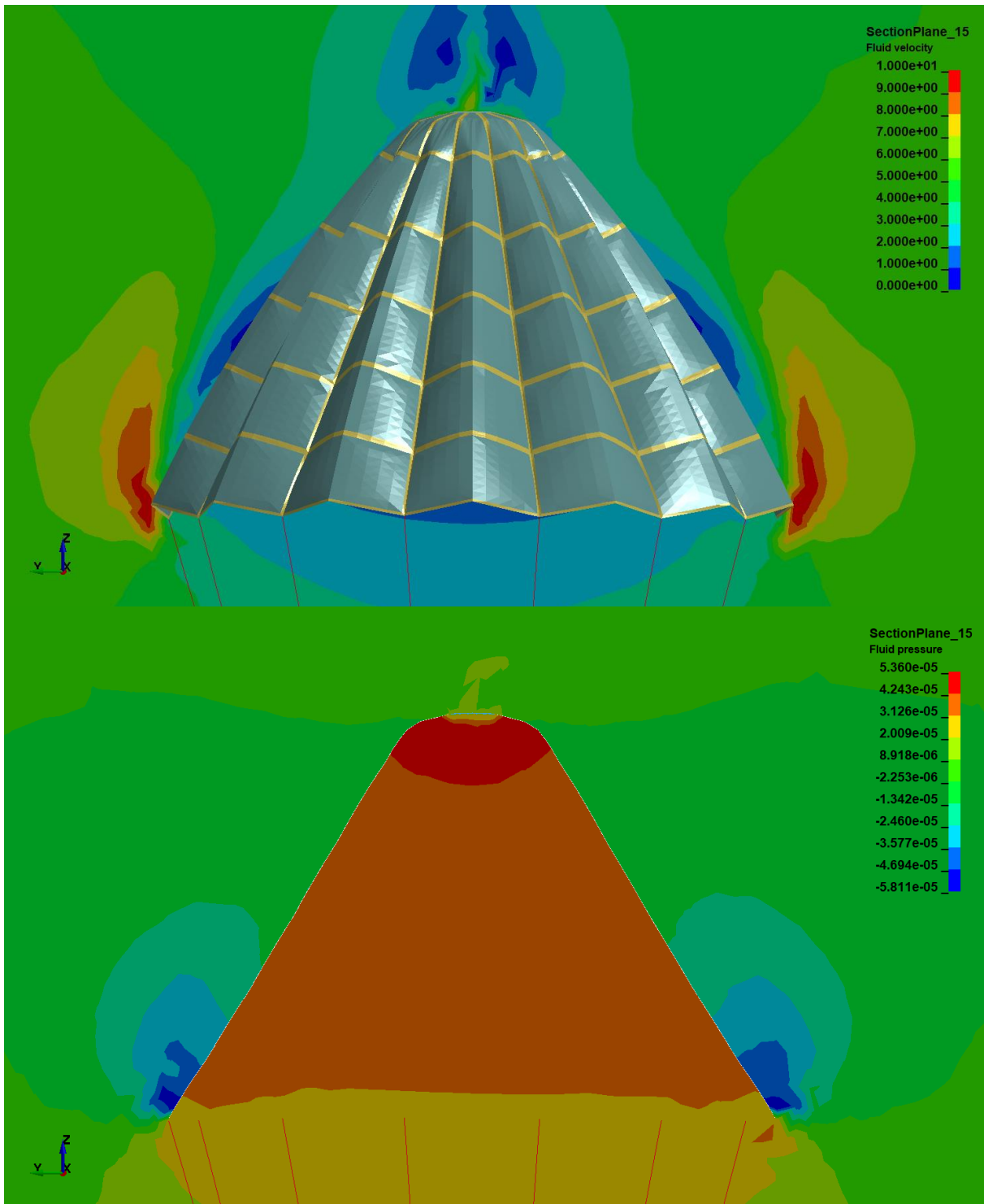


Fig.17: Velocity (top) and pressure (bottom) fields during FSI deployment at $t=160\text{ms}$

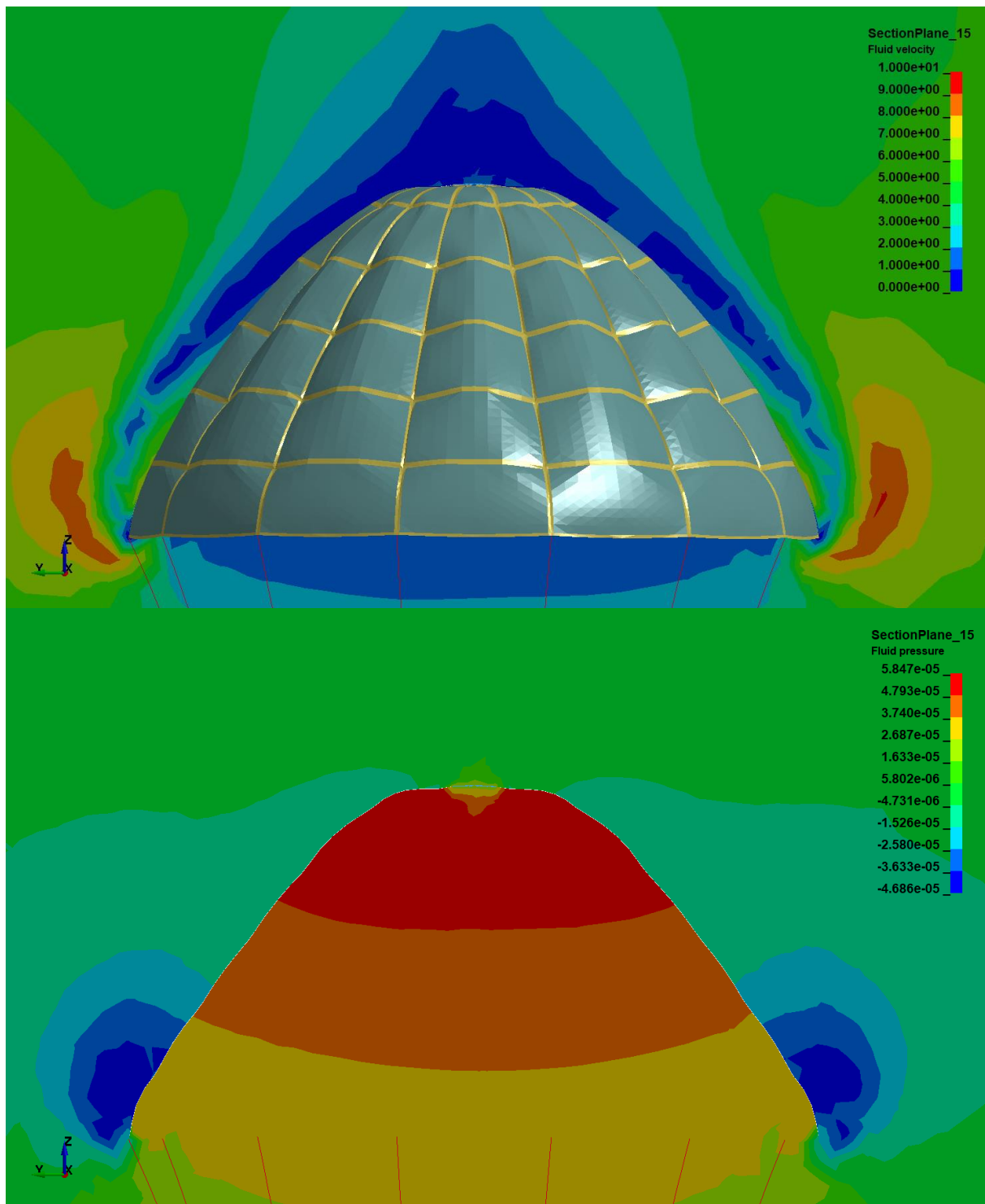


Fig. 18: Velocity (top) and pressure (bottom) fields during FSI deployment at $t=240\text{ms}$

6 Summary

This study permitted to describe all the methodologies associated with a parachute deployment calculation, from the choice of materials most suited to the available fabric data, to the folding procedure, and finally to the calibration of both implicit dynamics and ICFD aspects of the problem.

These methodologies were successfully applied to a 2m parachute test case, with increasing complexity. The ICFD solver demonstrated its robustness and its ability to follow rapidly deformable structures. The demonstrator case shows its capacity to unfold with a fully coupled ICFD simulation, including fluid permeability through the porous fabric using new thin structures features.

Improvements in the modelling are necessary for deployment calculations starting from a more tightly folded configuration. In particular, adjustment of the mesh size of the coupled surface and ICFD mesh tuning are needed in order to ensure good mesh generation and pressure field calculation.

The way forward is to simulate the drop of a “pinetree” parachute in a still fluid domain. Present results are encouraging for the ICFD capability of such computations, especially in combination with results from [8] where rigid bodies were dropped in similar situations.

For validation purposes, an actual test case would be necessary, with load measurements at the bottom of the lines during deployment.

7 Literature

- [1] Coquet Y., Bordenave P., Capmas G., Espinosa C., Improvements in fluid structure interaction simulation of parachute using LS-DYNA, 21st AIAA, 2011-2590.
- [2] Tutt B., Charles R. D., Roland S., Noetscher G., Development of parachute simulation techniques in LS-DYNA, 11th International LS-DYNA Users Conference, 2012.
- [3] McQuilling M., Potvin J., Riley J., Simulating the Flows About Cargo Containers Used During Parachute Airdrop Operations, 28th AIAA Applied Aerodynamics Conference, Chicago, IL, June 28 - July 1, 2010
- [4] Desabrais K. J., Aerodynamic Forces on an Airdrop Platform, 18th AIAA, 2005-1634.
- [5] Clift R., Grace J.R. and Weber M.E., Bubbles, drops and particles, Academic Press, 1978
- [6] Loeser T., Bergmann A., Capabilities of Deployment Tests at DNW-NWB, Fluid Dynamics of Personnel and Equipment Precision Delivery from Military Platforms (pp. 10-1 to 10-12), 2006
- [7] Michel C., Grippon E., Seulin M., Lapoujade V., Freefall movement decomposition of a payload released by aircraft: study of aerodynamic coefficients using the LS-DYNA ICFD solver, 11th European LS-DYNA Conference, 2017
- [8] Le Garrec M., Seulin, M., Lapoujade V., Airdrop sequence simulation using LS-DYNA® ICFD solver and FSI coupling, 15th International LS-DYNA Users Conference, 2018
- [9] Hoerner, S. F., Fluid-Dynamic Drag, 1965